JPE 19-1-20

https://doi.org/10.6113/JPE.2019.19.1.211
ISSN(Print): 1598-2092 / ISSN(Online): 2093-4718

Three-coil Magnetically Coupled Resonant Wireless Power Transfer System with Adjustable-position Intermediate Coil for Stable Transmission Characteristics

Xuling Chen†, Lu Chen**, Weiwei Ye**, and Weipeng Zhang*

†,*College of Mechanical and Electrical Eng., Nanjing University of Aeronautics and Astronautics, Nanjing, China
**College of Automation Eng., Nanjing University of Aeronautics and Astronautics, Nanjing, China

Abstract

In magnetically coupled resonant (MCR) wireless power transfer (WPT) systems, the introduction of additional intermediate coils is an effective means of improving transmission characteristics, including output power and transmission efficiency, when the transmission distance is increased. However, the position of intermediate coils in practice influences system performance significantly. In this research, a three-coil MCR WPT system is adopted as an exemplification for determining how the spatial position of coils affects transmission characteristics. With use of the fundamental harmonic analysis method, an equivalent circuit model of the system is built to reveal the relationship between the output power, the transmission efficiency, and the spatial scales, including the axial, lateral, and angular misalignments of the intermediate and receiving coils. Three cases of transmission characteristics versus different spatial scales are evaluated. Results indicate that the system can achieve relatively stable transmission characteristics with deliberate adjustments in the position of the intermediate and receiving coils. A prototype of the three-coil MCR WPT system is built and analyzed, and the experimental results are consistent with those of the theoretical analysis.

Key words: Intermediate coil, Magnetically coupled resonant, Spatial scales, Stable transmission characteristics, Wireless power transfer

I. INTRODUCTION

The concept of wireless power transfer (WPT) based on magnetic coupling theory was proposed by Nikola Tesla more than a century ago [1]. WPT uses magneto-quasistatic fields to transfer energy over short to medium distances and has been increasingly applied in electric vehicles, consumer electronics, and implantable medical devices due to its superiority and usability in humid and lousy environments [2]-[4].

Manuscript received Aug. 31, 2018; accepted Oct. 18, 2018
Recommended for publication by Associate Editor Fuxin Liu.
†Corresponding Author: chenxuling@nuaa.edu.cn
Tel: +86-2584892501, Nanjing Univ. of Aeronautics and Astronautics
*Col. Mechanic. Electr. Eng., Nanjing Univ. Aeronautics Astronautics, China
**Col. Autom. Eng., Nanjing Univ. Aeronautics Astronautics, China

Magnetically coupled resonant (MCR) WPT technology can deliver power efficiently over medium distances [5]. The basic MCR WPT system usually consists of two coils, namely, transmitting and receiving coils, which operate at the same resonant frequency. Numerous studies have focused on the analysis, design, and optimization of the basic two-coil MCR WPT system [6]-[8], whose output power and transmission efficiency noticeably drop with increased transfer distance [9] or the variation of position in space [10], [11].

For further enhancement of transmission characteristics, intermediate coils were introduced between the transmitting and receiving coils of the MCR WPT system in previous works. Three- and four-coil MCR WPT systems have been extensively proposed for increasing output power and transmission efficiency, particularly in long-distance applications [12], [13]. Similar to the position of coils in a two-coil WPT

system, that in a three-coil WPT system considerably influences the transmission characteristics. Studies have been conducted to reveal the effect of intermediate coil on the performance of a system. [14] showed that three-coil inductive links can significantly improve transmission efficiency, particularly at long coupling distances, by transforming any arbitrary load impedance to the optimal impedance required at the input of the inductive link. The transmission efficiency of WPT with an intermediate coil was analyzed in [15], and the results showed that the intermediate resonant system had good transmission efficiency and was superior to nonintermediate systems. [16] discovered that placing an intermediate coil slightly near the transmission coil achieved better transmission efficiency than placing it slightly near the receiving coil. In [17], a three-coil WPT system structure was proposed and proven capable of significantly reducing the electromagnetic field emission caused by coil misalignment. In [18], the influence of spatial scales on the output power of three-coil system was investigated, but only one variable spatial scale was analyzed, meanwhile, the transmission efficiency was not considered.

In this paper, the transmission characteristics of a three-coil MCR WPT system versus the spatial scales, including axial, lateral, and angular misalignments, are discussed for stabilizing the output power and transmission efficiency at varying positions of the intermediate and receiving coils. Section II describes the basic theories and the key parameters of the three-coil MCR WPT system. According to equivalent circuit theory, the circuit model of the three-coil MCR WPT system is built, and the expressions of the output power and transmission efficiency are derived by the fundamental harmonic analysis (FHA) method. In Section III, the transmission characteristics of the system are analyzed and illustrated when the mutual inductances between the three coils are proportional. We find that the robustness of the output power and the transmission efficiency can be improved by an adjustment in the position of the intermediate coil according to the receiving coil. A prototype of the three-coil MCR WPT system is built and tested to validate the theoretical analysis in Section IV, which is followed by the conclusion in Section V.

II. Modeling and Analysis of Transmission Characteristics

Fig. 1 shows the circuit diagram of the three-coil MCR WPT system, which includes a half-bridge inverter; a voltage doubler rectifier; and three resonant coils, namely, the transmitting, intermediate, and receiving coils. The mutual inductances between two adjacent coils are defined as M_{12} and M_{23}, and the mutual inductance between transmitting and receiving coils is ignored for simplification. The input voltage is inverted by the half-bridge inverter and employed to drive

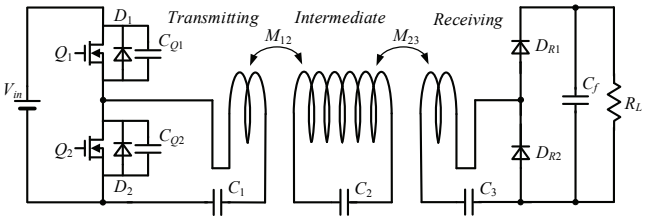

Fig. 1. Configuration of the three-coil MCR WPT system.

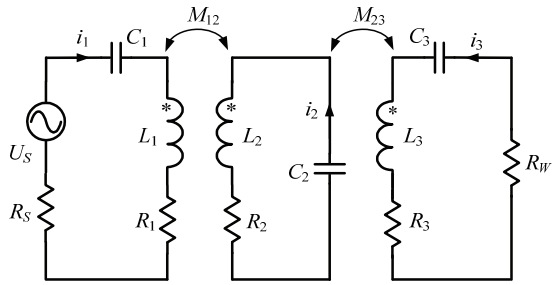

Fig. 2. Equivalent circuit of the system.

the resonant coils. Q_1 and Q_2 are the power switches driven in a complementary manner with the same duty cycle.

Fig. 2 shows the equivalent circuit of the three-coil MCR WPT system, where U_s is the equivalent alternating voltage source, L_1–L_3 are the self-inductances of the resonant coils, with parasitic resistances R_1–R_3. C_1–C_3 are the series resonant capacitors designed to resonate with L_1–L_3. R_S is the impedance of the AC voltage source. R_W is the equivalent load resistance.

For the half-bridge configuration, the norm of $\dot{U}_s$ can be calculated as

$$U_S = \left\|\dot{U}_S\right\| = \frac{\sqrt{2}}{\pi} V_{in}. \tag{1}$$

The equivalent load resistance (R_W) can be expressed by the load resistance (R_L) as

$$R_W = \frac{2}{\pi^2} R_L. \tag{2}$$

The resonant frequency is defined as

$$f_r = 1 \Big/ \left(2\pi\sqrt{L_r \cdot C_r}\right), \tag{3}$$

where L_r and C_r are the resonant inductor and capacitor, respectively. If the three-coil MCR WPT system operates in a resonant state, then $L_1 = L_2 = L_3 = L_r$, and $C_1 = C_2 = C_3 = C_r$.

According to Fig. 2 and Kirchhoff's voltage law, the following can be obtained:

$$\begin{bmatrix} R_S + R_1 & j\omega M_{12} & 0 \\ j\omega M_{12} & Z_2 & j\omega M_{23} \\ 0 & j\omega M_{23} & R_3 + R_W \end{bmatrix} \begin{bmatrix} \dot{I}_1 \\ \dot{I}_2 \\ \dot{I}_3 \end{bmatrix} = \begin{bmatrix} \dot{U}_S \\ 0 \\ 0 \end{bmatrix}, \tag{4}$$

where $\omega = 2\pi f_r$, and $\dot{I}_1 - \dot{I}_3$ are the fundamental harmonics of the resonant currents.

If $R_{1S} = R_1 + R_S$ and $R_{3W} = R_3 + R_W$, then $\dot{I}_1 - \dot{I}_3$ can be solved from (4).

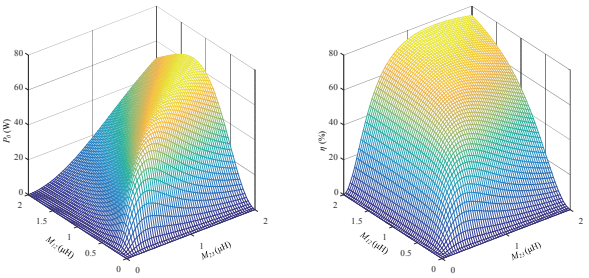

(a) (b)

Fig. 3. 3D graphs of P_o and η versus M_{12} and M_{23}: (a) P_o; (b) η.

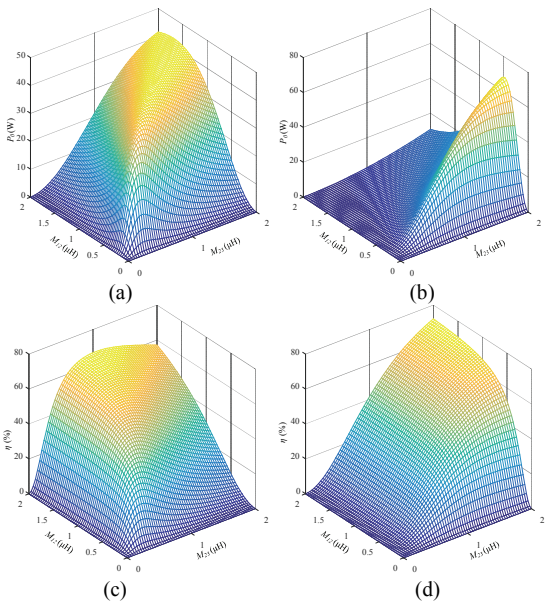

(a) (b)

(c) (d)

Fig. 4. Transfer characteristics under different loads: (a) P_o (R_L = 2 Ω); (b) P_o (R_L = 50 Ω); (c) η (R_L = 2 Ω); (d) η (R_L = 50 Ω).

$$\begin{cases} \dot{I}_1 = \dfrac{U_S(\omega^2 M_{23}^{\ 2} + R_2 R_{3W})}{\omega^2 M_{12}^{\ 2} R_{3W} + \omega^2 M_{23}^{\ 2} R_{1S} + R_{1S} R_2 R_{3W}} \\ \dot{I}_2 = \dfrac{-jU_S \omega M_{12} R_{3W}}{\omega^2 M_{12}^{\ 2} R_{3W} + \omega^2 M_{23}^{\ 2} R_{1S} + R_{1S} R_2 R_{3W}} \\ \dot{I}_3 = \dfrac{-U_S \omega^2 M_{12} M_{23}}{\omega^2 M_{12}^{\ 2} R_{3W} + \omega^2 M_{23}^{\ 2} R_{1S} + R_{1S} R_2 R_{3W}} \end{cases} \tag{5}$$

Therefore, the output power of the system P_o can be expressed as

$$P_o = \frac{U_S^{\ 2} \omega^4 M_{12}^{\ 2} M_{23}^{\ 2} R_W}{\left(\omega^2 M_{12}^{\ 2} R_{3W} + \omega^2 M_{23}^{\ 2} R_{1S} + R_{1S} R_2 R_{3W}\right)^2} \tag{6}$$

Radiation and power losses are ignored for simplification. Thus, the transmission efficiency η can be derived as

$$\eta = \frac{\omega^4 M_{12}^{\ 2} M_{23}^{\ 2} R_W}{(\omega^2 M_{23}^{\ 2} + R_2 R_{3W})\left(\omega^2 M_{12}^{\ 2} R_{3W} + \omega^2 M_{23}^{\ 2} R_{1S} + R_{1S} R_2 R_{3W}\right)} \tag{7}$$

From (6) and (7), the 3D graphs of the output power and the transmission efficiency versus M_{12} and M_{23} are illustrated in Fig. 3, and the specifications are as follows: V_{in} = 24 V, f_s = f_r = 200 kHz, R_S = 0.1 Ω, R_L = 5 Ω, R_1 = 0.093 Ω, R_2 = 0.21 Ω, and R_3 = 0.093 Ω. The values of R_1–R_3 are measured by the impedance network analyzer and adjusted according to the experimental results. Fig. 3 indicates that P_o and η are sensitive to variations in M_{12} and M_{23} and P_o and η generally decrease with M_{12} and M_{23}.

In realistic applications, R_L always changes. Fig. 4 plots how R_L influences P_o and η, from which we can conclude that P_o decreases with an increase in R_L in a specific variation range of M_{12} (or M_{23}). However, the variation of R_L has less influence on η compared with that of P_o. For simplification, the following analysis is based on a constant R_L (5 Ω).

III. Analysis of Spatial Scales for Stable Output Power and Transmission Efiffiency

As transmission characteristics are subject to the variation of mutual inductances in a three-coil MCR WPT system, the possibility of achieving stable transmission characteristics by the adjustment of mutual inductances should be determined.

Fig. 5 shows the contour lines extracted from Fig. 3 by the insertion of horizontal planes into Fig. 3 with different magnitudes that represent diverse transfer characteristics, from which we can conclude that P_o and η can remain stable within specific ranges if M_{12} is proportional to M_{23}.

If $M_{23} = k \cdot M_{12}$ and k is the proportional coefficient, then (6) can be simplified as

$$P_o = \frac{1}{\left(a_1 + \dfrac{a_2}{M_{12}^2}\right)^2} \tag{8}$$

$$\begin{cases} a_1 = \dfrac{R_{1S}}{U_S\sqrt{R_W}} \cdot k + \dfrac{R_{3W}}{U_S\sqrt{R_W}} \cdot \dfrac{1}{k} \\ a_2 = \dfrac{R_{1S} R_2 R_{3W}}{U_S \omega^2 \sqrt{R_W}} \cdot \dfrac{1}{k} \end{cases}, \tag{9}$$

and (7) can be simplified as

$$\eta = \frac{1}{\dfrac{b_1 b_3}{M_{12}^4} + \dfrac{b_1 b_4 + b_2 b_3}{M_{12}^6} + \dfrac{b_2 b_4}{M_{12}^8}} \tag{10}$$

$$\begin{cases} b_1 = \dfrac{1}{\omega^2 R_W} \\ b_2 = \dfrac{R_2 R_{3W}}{\omega^4 R_W} \cdot \dfrac{1}{k^2} \\ b_3 = \dfrac{R_{1S}}{\omega^2 R_W} \cdot k^2 + \dfrac{R_{3W}}{\omega^2 R_W} \cdot \dfrac{1}{k^2} \\ b_4 = \dfrac{R_{1S} R_2 R_{3W}}{\omega^4 R_W} \cdot \dfrac{1}{k^2} \end{cases}, \tag{11}$$

where a_1, a_2, b_1, b_2, b_3, and b_4 are constants related to the system parameters and k.

Based on (8)-(11) and $M_{23} = k \cdot M_{12}$, two clusters of curves of P_o and η versus M_{12} are illustrated in Fig. 6, which infers that coefficient k considerably influences P_o and η. If k is

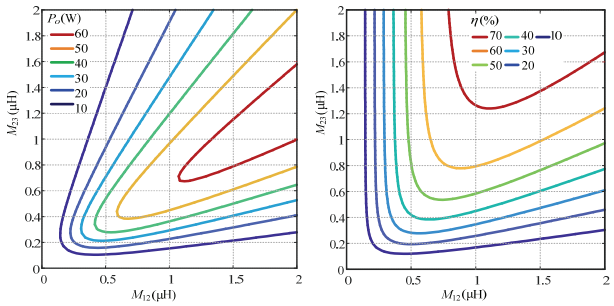

(a) (b)

Fig. 5. Contour with various mutual inductances: (a) P_o; (b) η.

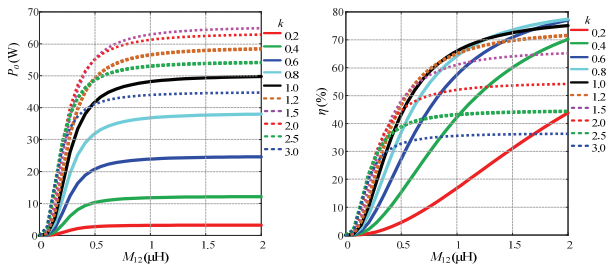

(a) (b)

Fig. 6. Curves of P_o and η versus M_{12}: (a) P_o; (b) η.

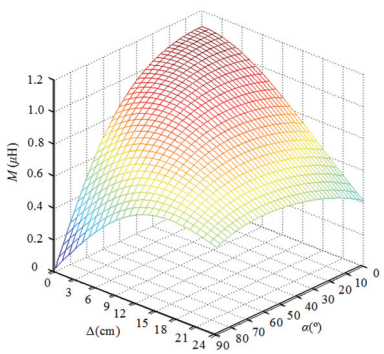

Fig. 7. 3D graphs of mutual inductance versus lateral and angular misalignments.

designed appropriately (for example, $k \geq 1$), then P_o and η will be nearly stable within a specific range of M_{12}. Theoretically, k can be random in practice, as shown in Fig. 6. To simplify the analysis, we select $k = 1$.

To further investigate the requirements on spatial scales to achieve stable transmission characteristics, the relationships between mutual inductances and spatial scales are first obtained [19]. Fig. 7 illustrates the behavior of mutual inductance under lateral and angular misalignments and indicates that misalignments substantially affect mutual inductance. With the substitution of the mutual inductance into (8) and (10), the tendency of P_o and η versus the spatial scales can be determined.

Case 1: One variable spatial scale

In this study, three typical spatial scales are considered in the following analysis, namely, the axial misalignment (d), the lateral misalignment (Δ), and the angular misalignment (α), as shown in Fig. 8. Meanwhile, three different cases are discussed, namely, one-, two-, and three-variable spatial scales. The specifications are given as follows: $r_1 = r_2 = r_3 = 0.11$ m, $N_1 = N_3 = 6$, and $N_2 = 14$.

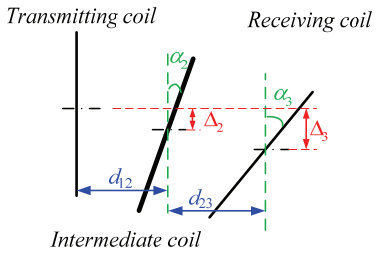

Fig. 8. Coil layout with axial, lateral, and angular misalignments.

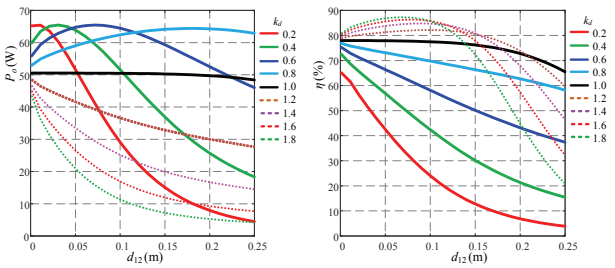

(a) (b)

Fig. 9. Curves of P_o and η versus d_{12}: (a) P_o; (b) η.

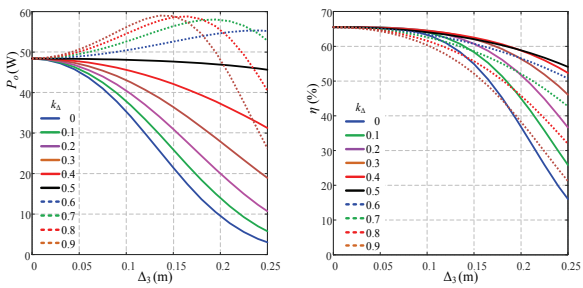

(a) (b)

Fig. 10. Curves of P_o and η versus Δ_3: (a) P_o; (b) η.

1) Axial Misalignment d (Δ = 0, α = 0)

With the assumption that $d_{23} = k_d \cdot d_{12}$, Fig. 9 shows the clusters of curves of P_o and η versus d_{12} under different k_d values. A remarkable discrepancy exists between the curves with different k_d values, and most curves fluctuate on a large scale. When $k_d = 1$ ($M_{23} = M_{12}$), the variation of P_o and η is relatively minor within the specific range of d_{12} ($0 \leq d_{12} \leq 0.2$ m), which means that the transmission characteristics of the system are approximately constant. However, if $k_d \neq 1$ or $d_{12} > 0.2$ m, then P_o and η will fluctuate severely, which is detrimental to providing a stable power for loads.

2) Lateral Misalignment Δ (d = 0, α = 0)

With the assumption that $\Delta_2 = k_\Delta \cdot \Delta_3$, Fig. 10 illustrates how k_Δ affects the tendency of P_o and η under different Δ_3 values. We can infer that P_o is more sensitive to k_Δ than η to k_Δ. Moreover, when $k_\Delta = 0.5$ ($M_{23} = M_{12}$), P_o and η decrease

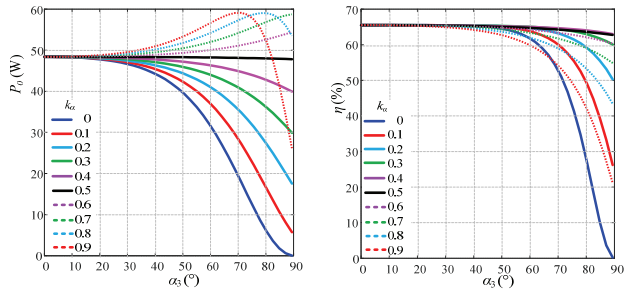

(a) (b)

Fig. 11. Curves of P_o and η versus α_3: (a) P_o; (b) η.

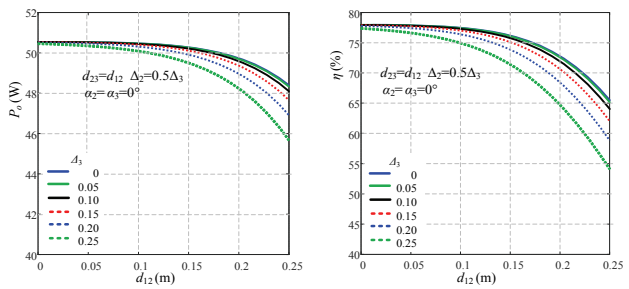

(a) (b)

Fig. 12. P_o and η versus d_{12} and Δ_3: (a) P_o; (b) η.

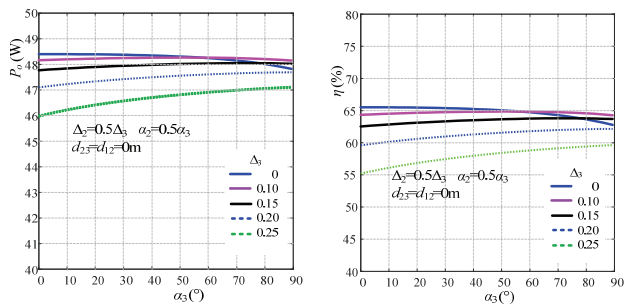

(a) (b)

Fig. 13. P_o and η versus Δ_3 and α_3: (a) P_o; (b) η.

slightly, which means that k_Δ=0.5 is also the best when only lateral misalignment is considered.

3) Angular Misalignment α (d = 0, Δ = 0)

With the assumption that $\alpha_2 = k_\alpha \cdot \alpha_3$, Fig. 11 illustrates the correlation between P_o, η, and α_3, where the maximal α_3 is supposed to be 90°. Compared with other curves, the ones when k_α equals 0.5 ($M_{23} = M_{12}$) are nearly constant over the full range of α_3, which means that if α_2 is strictly the half of α_3 ($0 \le \alpha_3 \le 90°$), then the system can always realize stable transmission characteristics.

From the above analysis, we can conclude that if only one spatial scale is considered, then a specific spatial range exists to keep the transmission characteristics of the three-coil MCR WPT system stable under the following conditions: $d_{23} = d_{12}$, $\Delta_2 = 0.5 \cdot \Delta_3$, or $\alpha_2 = 0.5 \cdot \alpha_3$.

Case 2: Two-variable spatial scales

Under the constraints of $d_{23} = d_{12}$, $\Delta_2 = 0.5 \cdot \Delta_3$, and $\alpha_2 = 0.5 \cdot \alpha_3$, the transmission characteristics of the three-coil MCR

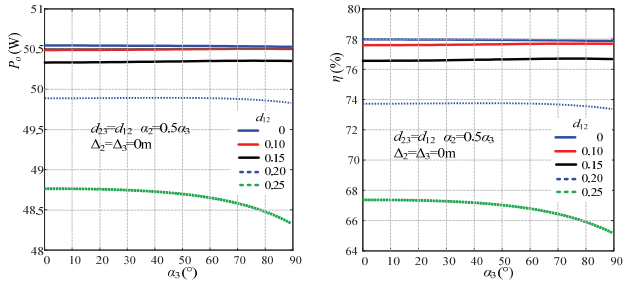

(a) (b)

Fig. 14. P_o and η versus Δ_3 and α_3: (a) P_o; (b) η.

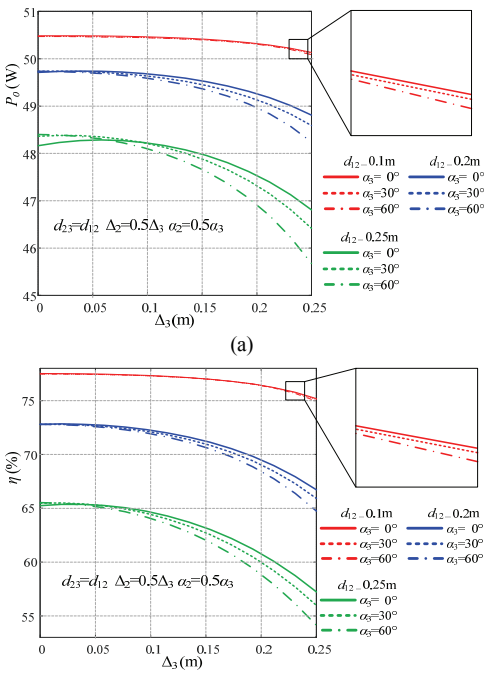

(a)

(b)

Fig. 15. P_o and η with axial, lateral, and angular misalignments: (a) P_o; (b) η.

WPT system when any two variable spatial scales are considered are analyzed as follows.

Figs. 12–14 demonstrate the curves of P_o and η versus d_{12}, Δ_3, and α_3. As shown in Fig. 12, P_o and η decrease with the increase of d_{12} and Δ_3. However, the transmission characteristics present less sensitivity to α than to d and Δ, as shown in Figs. 13 and 14. The spatial scale ranges for stable P_o and η are $d_{12} \le 0.2$ m, $\Delta_3 \le 0.25$ m, and $\alpha_3 \le 90°$ under the given specifications, which are consistent with those of the one-variable spatial scale.

Case 3: Three-variable spatial scales

Fig. 15 shows the curve clusters of P_o and η versus three spatial scales under the conditions of $d_{23} = d_{12}$, $\Delta_2 = 0.5 \cdot \Delta_3$, and $\alpha_2 = 0.5 \cdot \alpha_3$. The transmission characteristics decay with the increasing axial misalignment. In a specific range ($d_{12} \le$ 0.1 m), lateral and angular misalignments only slightly impact P_o and η; thus, the curves (red) are noticeably near each other and change smoothly. However, when $d_{12} >$ 0.1 m, P_o and η are

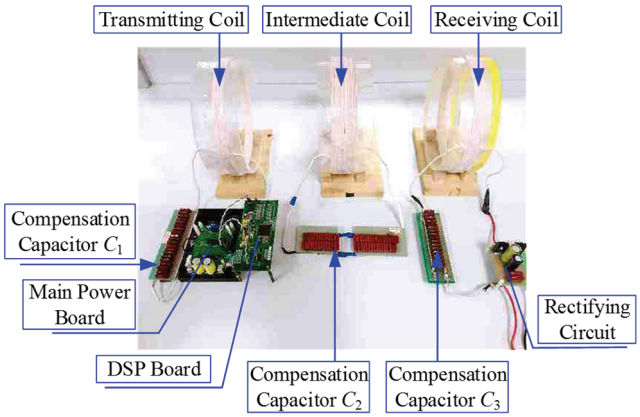

Fig. 16. Photo of the prototype.

TABLE I
SPECIFICATIONS OF THE SYSTEM

Parameters	Value	Parameters	Value
V_{in}	24 V	L_1	16.7 μH
R_S	0.1 Ω	L_2	66.87 μH
f_s	200 kHz	L_3	16.66 μH
r_1–r_3	11 cm	C_1	40.46 nF
N_1	6 turns	C_2	9.425 nF
N_2	14 turns	C_3	40.42 nF
N_3	6 turns	R_L	5 Ω

considerably influenced by lateral and angular misalignments, as shown by the blue and green curves. Meanwhile, axial and lateral misalignments have a greater influence on the transmission characteristics than does the angular misalignment.

From the analysis above, we can deduce that the three-coil MCR WPT system can realize a stable power transfer within a specific spatial scale range if the positions of the three coils are appropriately arranged to guarantee equal or proportional mutual inductances between two adjacent coils.

The misalignment range for stable P_o and η is not fixed because the transfer characteristics of the system depend on multiple parameters. Therefore, in practice, the misalignment range for stable P_o and η is determined by the specification of the system, especially by the proportional coefficient, k.

IV. EXPERIMENTAL VERIFICATION

To validate the theoretical analysis, a prototype of the three-coil MCR WPT system is built in the laboratory, as shown in Fig. 16, and the specifications are listed in Table I.

Figs. 17–19 show the theoretical and experimental results of the output power and transmission efficiency versus the one-variable spatial scales, respectively, where the solid curves represent the theoretical results and the dashed ones are the experimental data.

Figs. 20-22 illustrate the curves of the output power and transmission efficiency versus the two-variable spatial scales,

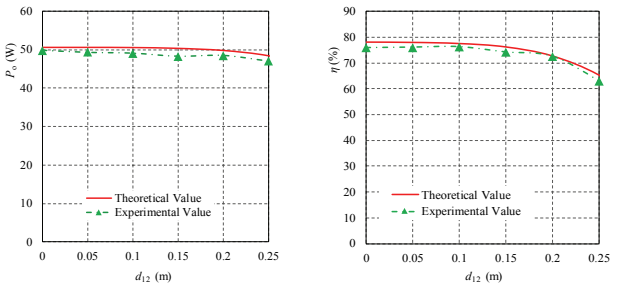

(a) (b)

Fig. 17. Theoretical and experimental data with different axial misalignments ($d_{12} = d_{23}$, $\Delta_2 = \Delta_3 = 0$ m, $\alpha_2 = \alpha_3 = 0°$): (a) P_o; (b) η.

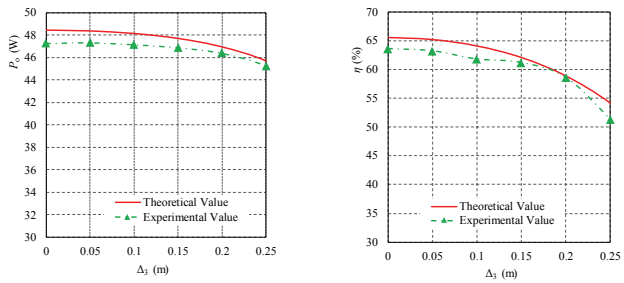

(a) (b)

Fig. 18. Theoretical and experimental data with different lateral misalignments ($d_{12} = d_{23} = 0.25$ m, $\Delta_2 = 0.5\ \Delta_3$, $\alpha_2 = \alpha_3 = 0°$): (a) P_o; (b) η.

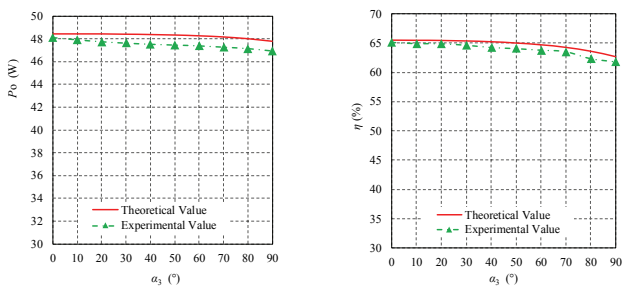

(a) (b)

Fig. 19. Theoretical and experimental data with different angular misalignments ($d_{12} = d_{23} = 0.25$ m, $\Delta_2 = \Delta_3 = 0$ m, $\alpha_2 = 0.5\ \alpha_3$): (a) P_o; (b) η.

respectively. The experimental results are also generally consistent with the theoretical results.

Fig. 23 demonstrates the output power and transmission efficiency at three spatial scales. As depicted, the angular misalignment has less effect on the transmission characteristics than do the axial and lateral misalignments; and this finding is consistent with the analysis in Section III.

Fig. 24 shows the key experimental waveforms under different spatial scales, where i_1 and i_3 are the currents of the transmitting and receiving coils, respectively. As shown in Fig. 24, the phase difference between i_1 and i_3 is 180°. Before the switch turns on, the drain current is negative, which indicates that the drain-to-source voltage (v_{ds}) is clamped to zero and the switch can achieve zero-voltage-switching.

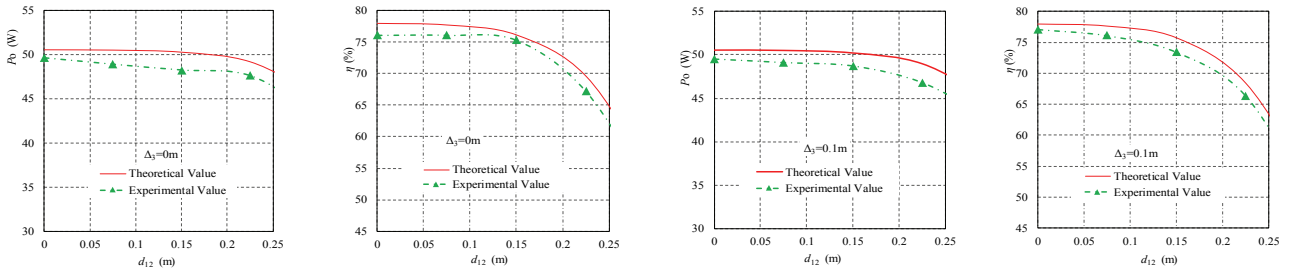

Fig. 20. Theoretical and experimental data with different axial and lateral misalignments ($d_{12} = d_{23}$, $\Delta_2 = 0.5\ \Delta_3$, $\alpha_2 = \alpha_3 = 0°$): (a) P_o ($\Delta_3 =$ 0 m); (b) η ($\Delta_3 = 0$ m); (c) P_o ($\Delta_3 = 0.1$ m); (d) η ($\Delta_3 = 0.1$ m).

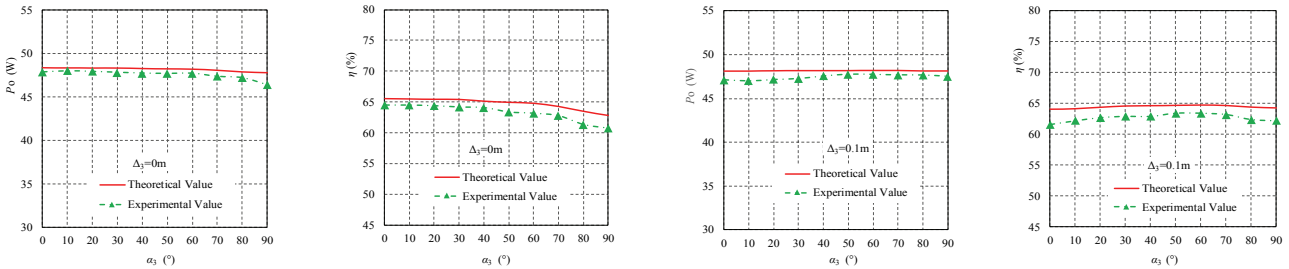

Fig. 21. Theoretical and experimental value with variant lateral and angular misalignments ($d_{12} = d_{23} = 0.25$ m, $\Delta_2 = 0.5\ \Delta_3$, $\alpha_2 = 0.5\ \alpha_3$): (a) P_o ($\Delta_3 = 0$ m); (b) η ($\Delta_3 = 0$ m); (c) P_o ($\Delta_3 = 0.1$ m); (d) η ($\Delta_3 = 0.1$ m).

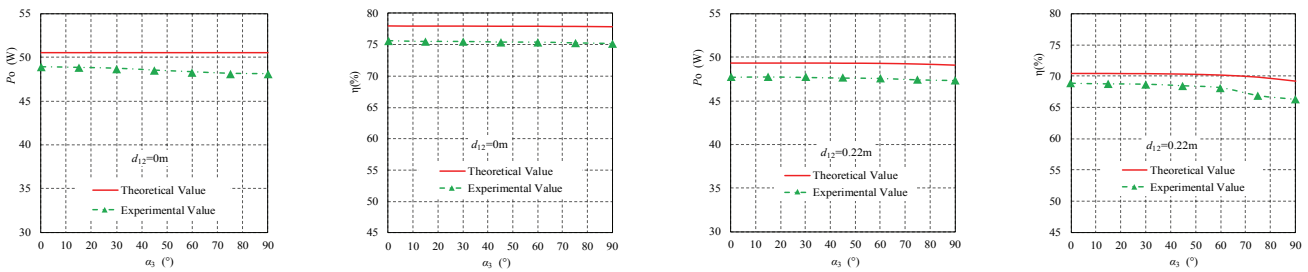

Fig. 22. Theoretical and experimental value with variant axial and angular misalignments: (a) P_o ($d_{12} = 0$ m); (b) η ($d_{12} = 0$ m); (c) P_o (d_{12} = 0.22 m); (d) η ($d_{12} = 0.22$ m).

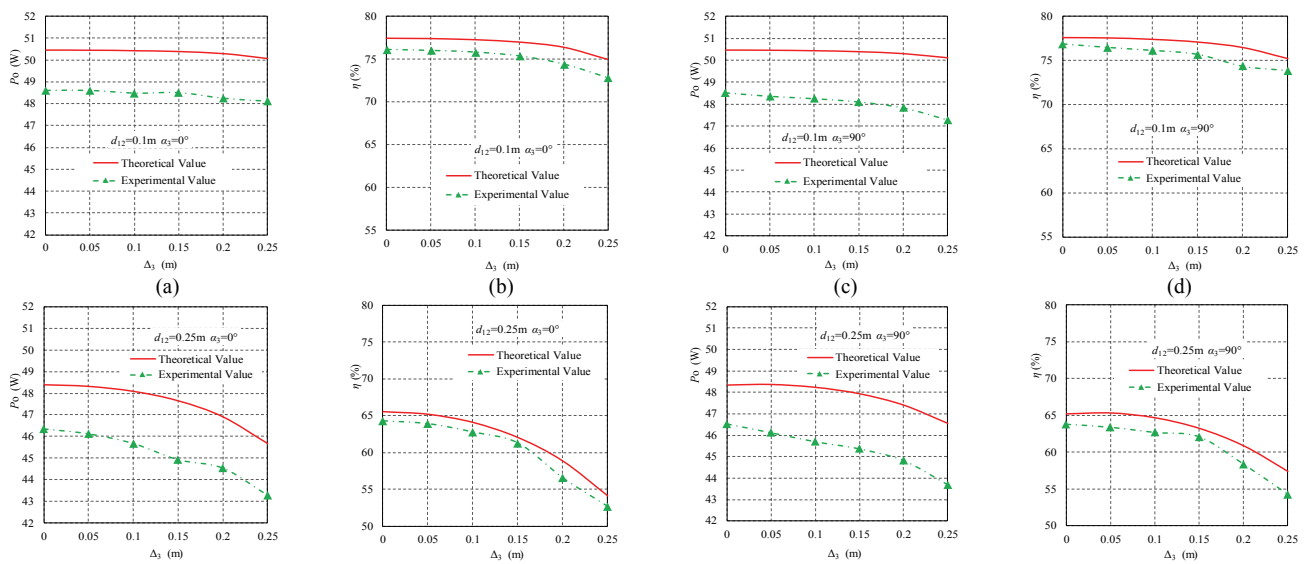

Fig. 23. Theoretical and experimental data with different axial, lateral and angular misalignments: (a) P_o (d_{12}=0.1m, α_3=0°); (b) η ($d_{12} =$ 0.1 m, $\alpha_3 = 0°$); (c) P_o ($d_{12} = 0.1$ m, $\alpha_3 = 90°$); (d) η ($d_{12} = 0.1$ m, $\alpha_3 = 90°$); (e) P_o ($d_{12} = 0.25$ m, $\alpha_3 = 0°$); (f) η ($d_{12} = 0.25$ m, $\alpha_3 = 0°$); (g) P_o ($d_{12} = 0.25$ m, $\alpha_3 = 90°$); (h) η ($d_{12} = 0.25$ m, $\alpha_3 = 90°$).

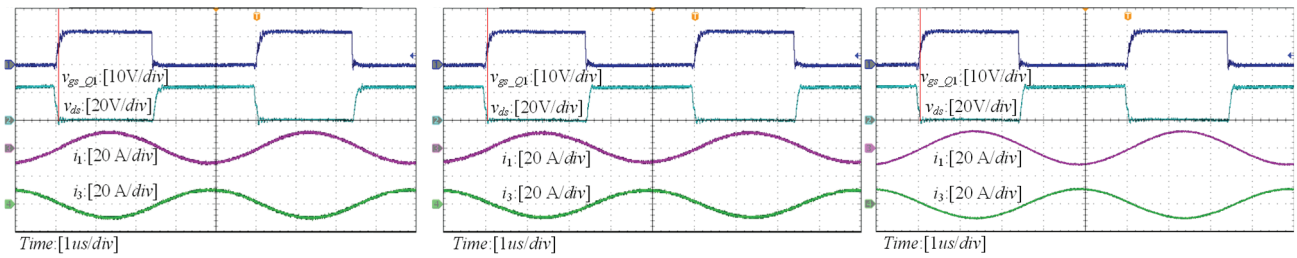

Fig. 24. Experimental waveforms: (a) Lateral misalignment ($\Delta_2 = 0.5\Delta_3 = 5$ cm, $\alpha_2 = \alpha_3 = 0°$); (b) Angular misalignment ($\Delta_2 = \Delta_3 = 0$ cm, $\alpha_2 = 0.5\alpha_3 = 10°$); (c) General misalignment ($\Delta_2 = 0.5\Delta_3 = 5$ cm, $\alpha_2 = 0.5\alpha_3 = 10°$).

V. Conclusions

This research investigates a three-coil MCR WPT system with transmitting, intermediate, and receiving coils. Via the equivalent circuit and FHA method, the output power and the transmission efficiency of the system with axial, lateral, and angular misalignments are analyzed in detail. We find that different spatial scales have varied influences on the transmission characteristics. Compared with axial and lateral misalignments, the angular misalignment has a minor impact on the system. By adjusting the position of the intermediate and receiving coils to ensure equal or proportional mutual inductances between two adjacent coils, the WPT system can achieve relatively stable transmission characteristics within a specific range of spatial scales. The conclusions are validated by experiments, whose results are consistent with those in the theoretical analysis.

Acknowledgment

This work was financially supported by the National Natural Science Foundation of China (51505223, 51877103), the Fundamental Research Funds for the Central Universities of China (NS2018020), the Natural Science Foundation of Jiangsu Province, China (BK20151471).

References

[1] L. I. Anderson, "Nikola Tesla on his work with alternating currents and their application to wireless telegraphy, telephony and transmission of Power," *Twenty First Century Books*, pp. 88-147, 2002.

[2] N. Shinohara, "Wireless power transmission progress for electric vehicle in Japan," in *Proc. IEEE Radio and Wireless Symposium*, pp. 109-111, 2013.

[3] S. Y. Hui, "Planar wireless charging technology for portable electronic products and Qi," in *Proc. IEEE*, Vol. 101, No. 6, pp. 1290-1301, Jun. 2013.

[4] L. Ho Yan, D. M. Budgett, and A. P. Hu, "Minimizing power loss in aircored coils for TET heart pump systems," *IEEE J. Emerg. Sel. Topics Circuits Syst.*, Vol. 1, No. 3, pp. 412-419, Sep. 2011.

[5] S. Y. R. Hui, W. X. Zhong, and C. K. Lee, "A critical review on recent progress in mid-range wireless power transfer," *IEEE Trans. Power Electron.*, Vol. 29, No. 9, pp. 4500-4511, Sep. 2014.

[6] M. W. Baker and R. Sarpeshkar, "Feedback analysis and design of RF power links for low-power bionic systems," *IEEE Trans. Biomed. Circuits Syst.*, Vol. 1, No. 1, pp. 28-38, Mar. 2007.

[7] Z. Yang, W. Liu, and E. Basham, "Inductor modeling in wireless links for implantable electronics," *IEEE Trans. Magn.*, Vol. 43, No. 10, pp. 3851-3860, Oct. 2007.

[8] U.-M. Jow and M. Ghovanloo, "Design and optimization of printed spiral coils for efficient transcutaneous inductive power transmission," *IEEE Trans. Biomed. Circuits Syst.*, Vol. 1, No. 3, pp. 193-202, Sep. 2007.

[9] J. O. Mur-Miranda, G. Fanti, Y. Feng, K. Omanakuttan, R. Ongie, A. Setjoadi, and N. Sharpe "Wireless power transfer using weakly coupled magnetostatic resonators," in *Proc. IEEE Energy Conversion Congress and Exposition (ECCE)*, pp. 4179-4186, 2010.

[10] Y. Lim, H. Tang, and S. Lim, "An adaptive impedance-matching network based on a novel capacitor matrix for wireless power transfer," *IEEE Trans. Power Electron.*, Vol. 29, No. 8, pp. 4403-4413, Aug. 2014.

[11] Z. Dang and J. Qahouq, "Modeling and investigation of magnetic resonance coupled wireless power transfer system with lateral misalignment," in *Proc. IEEE Applied Power Electronics Conference (APEC)*, pp. 1317-1322, 2014.

[12] J. W. Kim, H. C. Son, K. H. Kim, and Y. J. Park, "Efficiency analysis of magnetic resonance wireless power transfer with intermediate resonant coil," *IEEE Antennas Wireless Propag. Lett.*, Vol. 10, pp. 389-392, May 2011.

[13] M. Kiani, U. Jow, and M. Ghovanloo, "Design and optimization of a 3-coil inductive link for efficient wireless power transmission," *IEEE Trans. Biomed. Circuits Syst.*, Vol. 5, No. 6, pp. 579-591, Dec. 2011.

[14] M. Kiani, U. Jow, and M. Ghovanloo, "Design and optimization of a 3-coil inductive link for efficient wireless power transmission," *IEEE Trans. Biomed. Circuits Syst.*, Vol. 5, pp. 579-591, Dec. 2011.

[15] J. W. Kim, H. C. Son, K. H. Kim, and Y. J. Park, "Efficiency analysis of magnetic resonance wireless power transfer with intermediate resonant coil," *IEEE Antennas Wireless Propag. Lett.*, Vol. 10, pp. 389-392, 2011.

[16] D. J. Ahn and S. C. Hong, "A study on magnetic field repeater in wireless power transfer," *IEEE Trans. Ind. Electron.*, Vol. 60, No. 1, pp. 360-371, Jan. 2013.

[17] J. Zhang, X. Yuan, and C. Wang, "Comparative analysis of two-coil and three-coil structures for wireless power transfer," *IEEE Trans. Power Electron.*, Vol. 32, No. 1, pp.

341-352, Jan. 2017.
[18] W. Ye, L. Chen, F. Liu, X. Chen, and X. Wang, "Analysis and optimization of 3-coil magnetically coupled resonant wireless power transfer system for stable power transmission," *Proc. IEEE Energy Conversion Congress and Exposition (ECCE)*, pp. 2584-2589, 2017.
[19] A. P. Sample, D. A. Meyer, and J. R. Smith, "Analysis, experimental results, and range adaptation of magnetically coupled resonators for wireless power transfer," *IEEE Trans. Ind. Electron.*, Vol. 58, No. 2, pp. 544-554, Feb. 2011.

Xuling Chen was born in Hunan Province, China, in 1979. She received her B.S., M.S., and Ph.D. in mechanical and electrical engineering from the Nanjing University of Aeronautics and Astronautics (NUAA), Nanjing, China, in 2002, 2005, and 2011, respectively. In 2005, she joined the Faculty of the College of Automation Engineering, NUAA, where she is currently Lecturer. In 2017, she joined the Department of Electrical and Computer Engineering, Technical University of Munich, Munich, Germany, as Visiting Scientist. Her main research interests include wireless power transfer, mechanical and electrical engineering, and mechanical design.

Lu Chen was born in Jiangsu Province, China, in 1991. She received her B.S. and M.S in electrical engineering from NUAA, Nanjing, China, in 2014 and 2017, respectively. Her main research interests include parallel resonant converters and wireless power transfer.

Weiwei Ye was born in Jiangsu Province, China, in 1993. She received her B.S. in electrical engineering and automation from NUAA, Nanjing, China, in 2016, where she is working toward obtaining her M.S. in electrical engineering. Her main research interest is wireless power transfer.

Weipeng Zhang was born in Shanxi Province, China in 1994. He received his B.S. in mechanical and electrical engineering from Tianjin University of Science & Technology, Tianjin, China, in 2017. He is working toward acquiring his M.S. in mechanical and electrical engineering from NUAA, Nanjing, China. His present research interest is wireless power transfer.